

Exploring low temperature Li⁺ ion conducting plastic battery electrolyte

Avirup Das · Awalendra K. Thakur · K. Kumar

Received: 26 December 2012 / Revised: 25 March 2013 / Accepted: 27 March 2013 / Published online: 2 June 2013
© Springer-Verlag Berlin Heidelberg 2013

Abstract We report blend-based plastic polymer electrolyte (i.e., polyethylene oxide (PEO)–polydimethyl siloxane (PDMS)–lithium hexafluorophosphate (LiPF₆)) with substantial improvement in DC conductivity at ambient and subambient temperatures when compared with literature reports. Conductivity variation with salt concentration, investigated within ±30 °C range, indicates an optimum conductivity of 5.6×10^{-5} S cm⁻¹ at 30 °C for Ö/Li ~10 with a further lowering by one order at 0 °C and it remains unaltered at -10 °C. Enhanced conductivity in this blend electrolyte, though lower than two copolymer counterparts, is attributed to very low glass transition temperatures of the host polymers. X-ray diffraction (XRD) and scanning electron microscopy (SEM) suggest an effective blending between the two polymers with an effective interaction between the Li salt and the blend polymer matrix. Raman spectroscopy results indicated that cation (Li⁺) coordination occurs at the C=Ö site in PEO out of the two electron-rich sites (i.e., CÖ and Si-Ö-Si) in the PEO–PDMS blend. The blend electrolytes are predominantly ionic ($t_{\text{ion}} \sim 97\%$).

Keywords Plastic electrolyte · Low temperature · Conductivity · Ion transport · Battery

Introduction

Development of a suitable and stable electrolyte having desirable conductivity ($\sim 10^{-3}$ to 10^{-5} S cm⁻¹) at subambient temperatures for energy storage device applications has always been a great challenge. To achieve this target, intensive research has been taken up to develop appropriate ion-conducting separator component (electrolyte) with inherent features of high conductivity at low temperature and better stability (i.e., thermal, mechanical, voltage, etc.). Such desirable materials are of different types: (1) conventional liquid electrolytes, (2) gel/plasticized polymer electrolytes (PPE), and (3) dry solid polymer electrolytes (SPE). Liquid electrolytes formed by dissolution of appropriate Li salt in aprotic polar solvents (i.e.; binary/ternary/quaternary carbonates) have exhibited very high conductivity at low temperatures. Few important examples reported in literature are: lithium hexafluorophosphate (LiPF₆)–EMC (4×10^{-3} S cm⁻¹ at 30 °C, 4×10^{-3} S cm⁻¹ at 0 °C, 2×10^{-3} S cm⁻¹ at -20 °C) [1], LiF–PC–DMC–TPFPB (3.2×10^{-3} S cm⁻¹ at 20 °C, 2×10^{-3} S cm⁻¹ at 0 °C, 1.2×10^{-3} S cm⁻¹ at -20 °C) [2], LiBF₄–PC–DMC (1.8×10^{-3} S cm⁻¹ at -20 °C) [2], LiBOB–PC–EC–EMC (10^{-4} S cm⁻¹ at -30 °C) [3], LiPF₆–EC–DEC–EP (10^{-3} S cm⁻¹ at -30 °C) [4], LiPF₆–EC–DMC–EMC (2×10^{-3} S cm⁻¹ at -30 °C), LiPF₆–EC–DMC (2×10^{-3} S cm⁻¹ at -30 °C) [1], LiPF₆–EC–PC–EMC (10^{-3} S cm⁻¹ at -30 °C) [5], LiBF₄–PC–EC–EMC (10^{-3} S cm⁻¹ at -30 °C) [5], LiPF₆–EC–EMC (0.5×10^{-3} S cm⁻¹ at -50 °C) [6], etc. Most of nonaqueous polar solvents used in these electrolytes have low freezing points (EC=36.4 °C, DMC=2.4 °C, DEC=-43.0 °C, PC=-48.8 °C) [7] that it imparts them better conductivity even at low temperatures. However, main disadvantages of liquid electrolytes are chemical reactivity with lithium metal electrode, leakage

A. Das · A. K. Thakur · K. Kumar
Department of Physics, Indian Institute of Technology Kharagpur,
Kharagpur- 721302, India

A. K. Thakur (✉)
Department of Physics, Indian Institute of Technology Patna,
Patna 800013, India
e-mail: akt@iitp.ac.in

A. K. Thakur
e-mail: akt@phy.iitkgp.ernet.in

and degradation in performance at elevated temperatures, design flexibility, additional inert separator requirement for device fabrication, etc. In view of these difficulties, search for an alternative electrolyte that can serve the dual purpose of electrolyte as well as separator component at low temperatures has always been felt. The development of gel polymer electrolyte (GPE)/PPE was considered quite promising with possibility of replacement for organic liquid electrolytes by GPE. GPE exhibited DC conductivity in the range 10^{-3} – 10^{-5} S cm $^{-1}$ at subambient temperature limits. A lot of work on GPE with low temperature conductivity has been reported in literature. Few typical examples are: PAN–PMMA–EC–DMC–LiPF $_6$ (10^{-4} S cm $^{-1}$ at -10 °C) [8], PVDF–HFP–EC–DEC–LiN(CF $_3$ SO $_2$) $_2$ (10^{-5} S cm $^{-1}$ at -20 °C) [7], PMMA–DMF–PC–PWA (10^{-4} S cm $^{-1}$ at -30 °C) [9], PVDF–DMF–PWA (10^{-4} S cm $^{-1}$ at -30 °C) [9], etc. However, GPEs have their own limitations as battery/supercapacitor electrolytes that arise due to (1) the composition (e.g., prepared by dipping polymer films in a suitable solution comprising of salt and polar solvents like EC, PC, DMC, DEC, etc.) and (2) poor mechanical stability caused by the presence of polar solvents in the GPE matrix.

In view of the discussion mentioned above and features desirable for device applications, a solvent-free SPE appears to be a promising candidate for low temperature electrolyte provided the chosen polymer has a very low T_g in the subambient limit. Otherwise, a salt polymer complexed system generally does not show good DC conductivity at ambient (room) and subambient (low) temperatures. The literature reveals that conventional SPEs have very low conductivity that renders them unfit for use as a separator in battery. For example, polyethylene oxide (PEO)–LiPF $_6$ -based SPE shows conductivity $<10^{-7}$ S cm $^{-1}$ [10–12] at room temperature. It was previously reported [13] that 30 (wt.%) polydimethyl siloxane (PDMS) shows much better conductivity (8.7×10^{-4} S cm $^{-1}$) in PEO–PDMS–LiI system, whereas PEO–LiI system shows conductivity $\sim 10^{-6}$ S cm $^{-1}$ at 30 °C [13–15]. A comparison of low temperature conductivity for various classes of electrolyte is given in Fig. 1a and b as an illustration.

In order to enhance ambient and subambient conductivity in free-standing ion-conducting solid polymers, several approaches such as: (1) cross-linking, (2) blending, (3) addition of plasticizer, and (4) dispersion of filler [7], etc. have been implemented and evaluated. It is noted that a blend-based polymer electrolyte is relatively attractive because blending of two polymers with low and different glass transition temperatures (T_g) causes positive impact by: (1) improving mechanical property, (2) suppressing crystallinity, and (3) enhancing electrical conductivity. Such possibilities have, in fact, been found reasonably well in view of

earlier reports in literature. Fonseca et al. [16] and Johnstone et al. [17] reported that P(DMS-co-EO)–LiCLO $_4$ and P(DMS-co-EO)–MeSiCL $_3$ –LiCLO $_4$ systems exhibited conductivity as high as $\sim 10^{-4}$ S cm $^{-1}$ at room temperature, whereas a typical PEO–LiCLO $_4$ system shows a room temperature conductivity of $\sim 10^{-6}$ S cm $^{-1}$ [18]. Also, PDMS–PEG–LiTFSi [19] system shows conductivity of $\sim 10^{-4}$ S cm $^{-1}$. These examples clearly suggest that inclusion of PDMS in a polymer–salt complex system may be expected to enhance the ionic conductivity at room temperature as well as at subambient temperatures. At room temperature, PDMS exists in a gelly phase. So, inclusion of PDMS eventually changes the local viscosity of the polymer matrix, thereby reducing internal friction for ion migration and facilitating large enhancement in conductivity. This feasibility seems logical and reasonable in view of the liquidlike behavior of the polymer blend having very low T_g that favors local polymer chain motion even at lower temperatures and facilitates ion hopping from one available site to another such site in the host polymer backbone.

In the present work, PEO ($T_g \sim -65$ °C) and PDMS ($T_g \sim -120$ °C) blend has been used as the host matrix. Effect of salt (LiPF $_6$) concentration on conductivity of the polymer blend–salt complex has been investigated over a range of temperature in the subambient limit. The structural changes in the host polymer on complexation with salt have been investigated using x-ray diffraction (XRD) and scanning electron microscopy (SEM) analyses. Optimization of ionic conductivity with respect to salt concentration in the SPE over a temperature range of -30 to 30 °C has been studied and analyzed to explore the possibility of further scaling up of the optimized composition for device applications.

Experimental procedure

Polymer blend-based solid electrolyte separator films have been prepared by a standard solution cast technique reported elsewhere [20]. PEO (Sigma-Aldrich, Mw. $\sim 6 \times 10^5$) and PDMS (Alfa Aesar, Mw. $\sim 13,900$) were used to prepare polymer blend host matrix. LiPF $_6$ (Sigma-Aldrich) was chosen as the lithium salt and tetrahydrofuran (THF) was used as organic solvent. Polymers and the salt were dried and used without further purification. Initially, PEO and 30 wt.% of PDMS (with respect to PEO, w/w) was stirred mechanically in THF solvent for 10 h. This was done to carry out physical blending of the two polymers having different T_g in the subambient region. Subsequently, LiPF $_6$ was added in stoichiometric ratio (Ö/Li $\sim 10, 15, 20, 25,$ and 30) in to the polymer blend and stirred mechanically for 12 h to

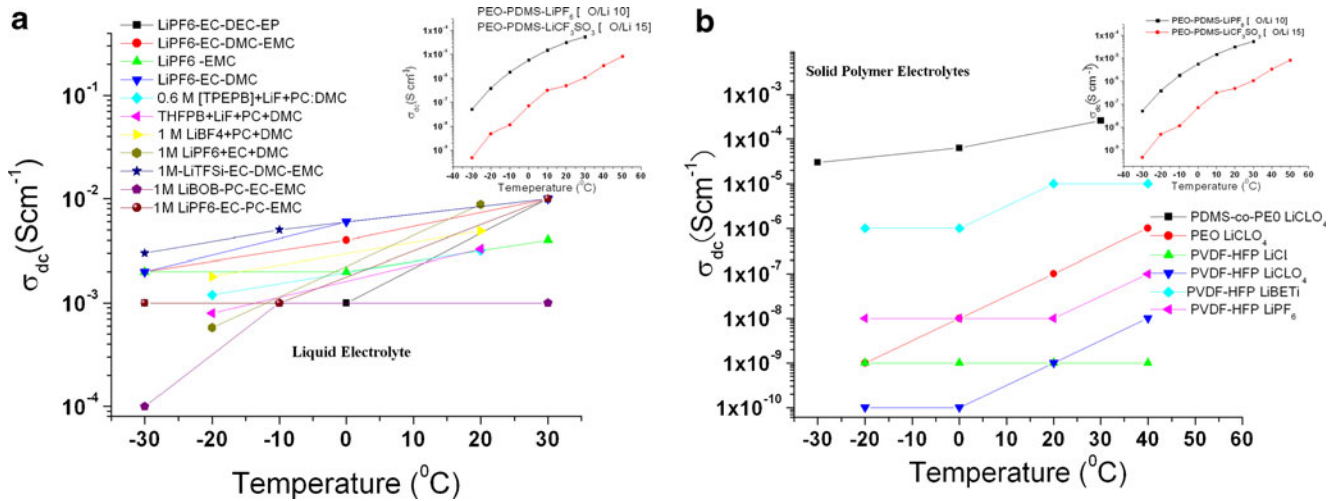


Fig. 1 **a** Conductivity comparison of liquid electrolyte at ambient (room) to subambient (below 0 °C) temperature range. **b** Conductivity comparison of solid electrolyte at ambient (room) to subambient (below 0 °C) temperature range. [1–6; 16, 18]

allow complexation. This stoichiometric (\ddot{O}/Li) ratio of salt has been calculated considering oxygen of PEO. The formula for this calculation has been shown below [20]:

$$\frac{\ddot{O}}{Li} = \frac{\text{No. of monomer unit in one gram of PEO}}{\text{No. of LiPF}_6 \text{ molecule in one gram of salt}} \times \frac{\text{wt. of PEO taken}}{\text{wt. of salt taken}} \quad (1)$$

Finally, the complexed polymer blend solution was cast in a glass Petri dish and kept in inert atmosphere for slow drying. Next, the free-standing polymer films so obtained have been characterized and evaluated for its suitability as a device component using various analytical techniques.

The XRD pattern of the series of samples with different salt concentrations has been recorded at room temperature

with an x-ray diffractometer (Rigaku, Japan), using $CuK\alpha$ radiation ($\lambda=1.5418 \text{ \AA}$) over a range ($4^\circ \leq 2\theta \leq 90^\circ$) of diffraction angle. The surface morphology of blend-based polymer electrolyte with variation of salt concentration has been studied by SEM. A differential scanning calorimetric (DSC) study has been carried out by PerkinElmer DSC 8000 setup. Thermograms have been recorded with a scan rate of $10^\circ/\text{min}$ in an inert atmosphere in a temperature range of -100 to $100 \text{ }^\circ\text{C}$. Raman spectrum of the polymer–salt complex films has been collected at room temperature ($27 \text{ }^\circ\text{C}$) using a micro-Raman spectrophotometer (Seki Technotron, Japan, model: STR 750). The experiment was performed using argon ion laser of wavelength (λ) $\sim 514 \text{ nm}$. Electrical property of the samples were measured with complex impedance spectroscopy on a symmetric cell: $Au | SPE || Au$ in the frequency range from 0.1 Hz to 1.0 MHz at an AC input signal $\sim 50.0 \text{ mV}$ (peak to peak) applied across the blocking electrodes.

Fig. 2 **a** X-ray diffraction pattern of pure PEO, PEO–PDMS (30 % w/w) blend, and PEO–PDMS (30 % w/w)– $LiPF_6$ with \ddot{O}/Li 10, 15, 20, 25, 30, and 35. **b** X-ray diffraction pattern of selected region for pure PEO, PEO–PDMS (30 % w/w) blend, and PEO–PDMS (30 % w/w)– $LiPF_6$

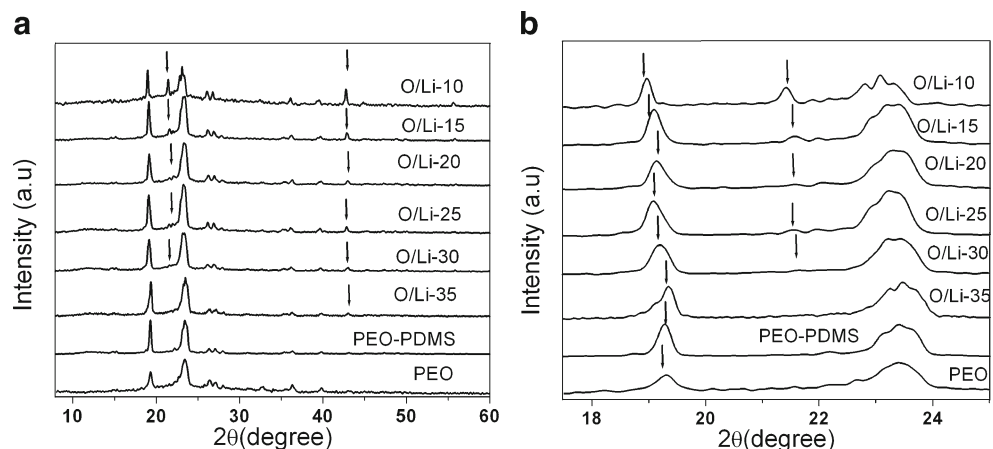


Table 1 X-ray diffraction and DC conductivity at ± 30 °C for SPE

Sample name	Peak position (2θ) (°)	d spacing (Å)	Interchain spacing (Å)	Conductivity ($S\ cm^{-1}$)	
				$T=30$ °C	$T=-30$ °C
PEO	19.3	4.598	5.748	–	–
PEO–PDMS	19.27	4.605	5.757	–	–
PEO–PDMS–LiPF ₆ [Ö/Li-10]	18.96	4.680	5.850	5.7×10^{-5}	5.7×10^{-8}
PEO–PDMS–LiPF ₆ [Ö/Li-15]	19.1	4.646	5.808	3.6×10^{-6}	5.6×10^{-11}
PEO–PDMS–LiPF ₆ [Ö/Li-20]	19.12	4.641	5.802	5.0×10^{-6}	1.9×10^{-10}
PEO–PDMS–LiPF ₆ [Ö/Li-25]	19.07	4.653	5.817	1.0×10^{-6}	9.9×10^{-12}
PEO–PDMS–LiPF ₆ [Ö/Li-30]	19.2	4.622	5.778	2.5×10^{-6}	1.9×10^{-11}
PEO–PDMS–LiPF ₆ [Ö/Li-35]	19.35	4.587	5.733	1.1×10^{-7}	–

The sample cell was kept inside a temperature chamber (Novocool) with facility of temperature variation in the range liquid nitrogen (LN_2) temperature to 250 °C. The

electrical impedance measurement for conductivity analysis in the present studies has been carried out in the temperature range 30 to -30 °C.

Fig. 3 SEM micrographs for a pure PEO, PEO–PDMS blend, and blend-based SPE with different Ö/Li

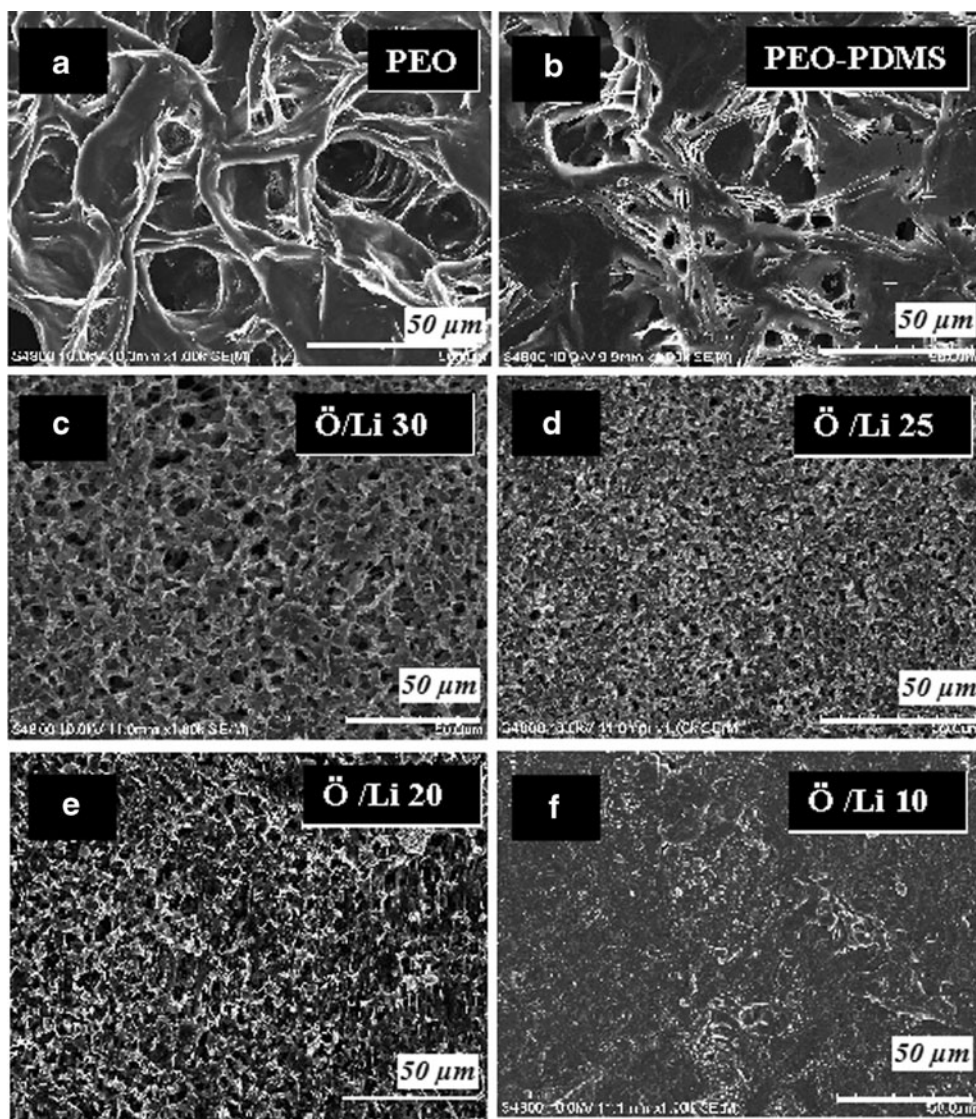
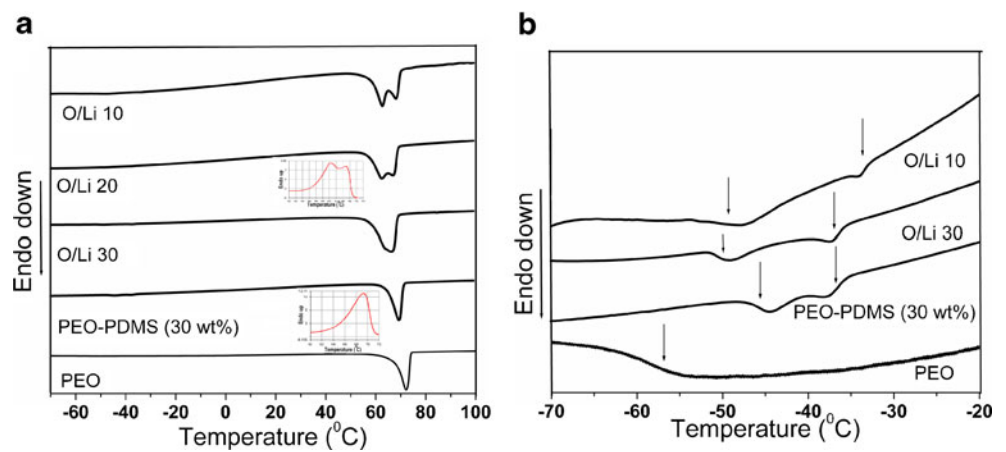


Fig. 4 **a** DSC pattern of PEO–PDMS (30 % w/w) blend and blend-based electrolyte (Ö/Li~ 10 and 30). **b** Glass transition of PEO–PDMS (30 % w/w) blend and blend-based electrolyte (Ö/Li~ 10 and 30)



Results and discussion

X-ray diffraction analysis

Figure 2a presents XRD pattern of pure PEO, PEO–PDMS blend, and blend salt complex with different stoichiometric ratios of blend salt composition expressed in terms of Ö/Li ratio. The characteristic XRD peak of PEO appears at ~19° and 23° [21]. They have been indexed in literature [21] as (120) and ((032) + (112)), respectively, for monoclinic crystal structure of PEO. On physical blending of PDMS with PEO, XRD pattern exhibits a noticeable change in terms of increase in the intensity of the characteristic PEO peaks. Additionally, a new peak (though weak) has also been noticed at 2θ ~22° along with broadening of the 23° peak of PEO–PDMS composition. These changes in the fingerprint XRD pattern of PEO confirm an affective blending with PDMS possibly due to interaction between the polymeric chains of PEO and PDMS on activation while stirring. No indication of phase separation could be noted. However, this observation needs to be corroborated further by additional evidence. It has been discussed in the next section.

When different stoichiometric ratios of salt (LiPF₆) are added to the PEO–PDMS blend, the XRD pattern exhibits clear changes. The noted changes are: (1) appearance of a new peak at 2θ ~43° for even the lowest salt content (Ö/Li ~35) that becomes stronger in intensity with increasing salt concentration (i.e., Ö/Li ~10) and (2) strength of

diffraction peak at 2θ ~22° attributed to PEO–PDMS blend increases with increasing salt concentration. The intensity of this peak is highest for Ö/Li ~10. This result provides another evidence for an effective interaction of Li⁺ salt with polymer blend, confirming the complexation of the polymer blend with salt in the free-standing polymer film. Further, both the 19° peak of PEO and 22° peak of PEO–PDMS have been noted to shift towards the lower diffraction angle side (Fig. 2b). Such a shift of the XRD peaks, on addition of salt in the polymer blend, indicates an enhancement in the interlayer (*d*) spacing of the host polymer structure. This change provides a convincing evidence for host polymer–salt complexation due to a strong interaction between the two entities. A clear broadening of the 23° peak of PEO has also been noted in the XRD pattern on inclusion of PDMS as well as salt in the host polymer matrix. This is attributed to the enhanced amorphous content, as expected. The changes in the intrinsic structural parameters (i.e., *d*-spacing and interchain separation of the polymer backbone that has greater significance in the case of noncrystalline/amorphous polymers) with variation in the salt concentration have been estimated using the following standard equations [20]:

$$d = \lambda / 2 \sin \theta \tag{2}$$

$$R = 5\lambda / 8 \sin \theta \tag{3}$$

where *d* is interlayer spacing, *R* is interchain separation, and λ is wavelength. The calculated values of *d* and *R* for

Table 2 Thermodynamic quantities of PEO, PEO–PDMS (30 % w/w) blend, and blend-based solid polymer electrolyte

Parameters → System↓	<i>T</i> _{g1} (°C)	<i>T</i> _{g2} (°C)	<i>T</i> ₁ (°C)	<i>T</i> ₂ (°C)	Normalized enthalpy (Δ <i>H</i> _m) (J/gm) w.r.t. PEO	Relative change in PEO crystallinity (%)
PEO	-58.0	–	72	–	199	92
PEO–PDMS (30 % w/w)	-46.0	-39.0	69	67	169	78
PEO–PDMS (30 % w/w)–LiPF ₆ (Ö/Li ~30)	-51.0	-37.5	66	63	169	78
PEO–PDMS (30 % w/w)–LiPF ₆ (Ö/Li ~20)	-49.0	-36.0	67	62	127	59
PEO–PDMS (30 wt.%)–LiPF ₆ (Ö/Li ~10)	-48.0	-35.0	68	62	67	31

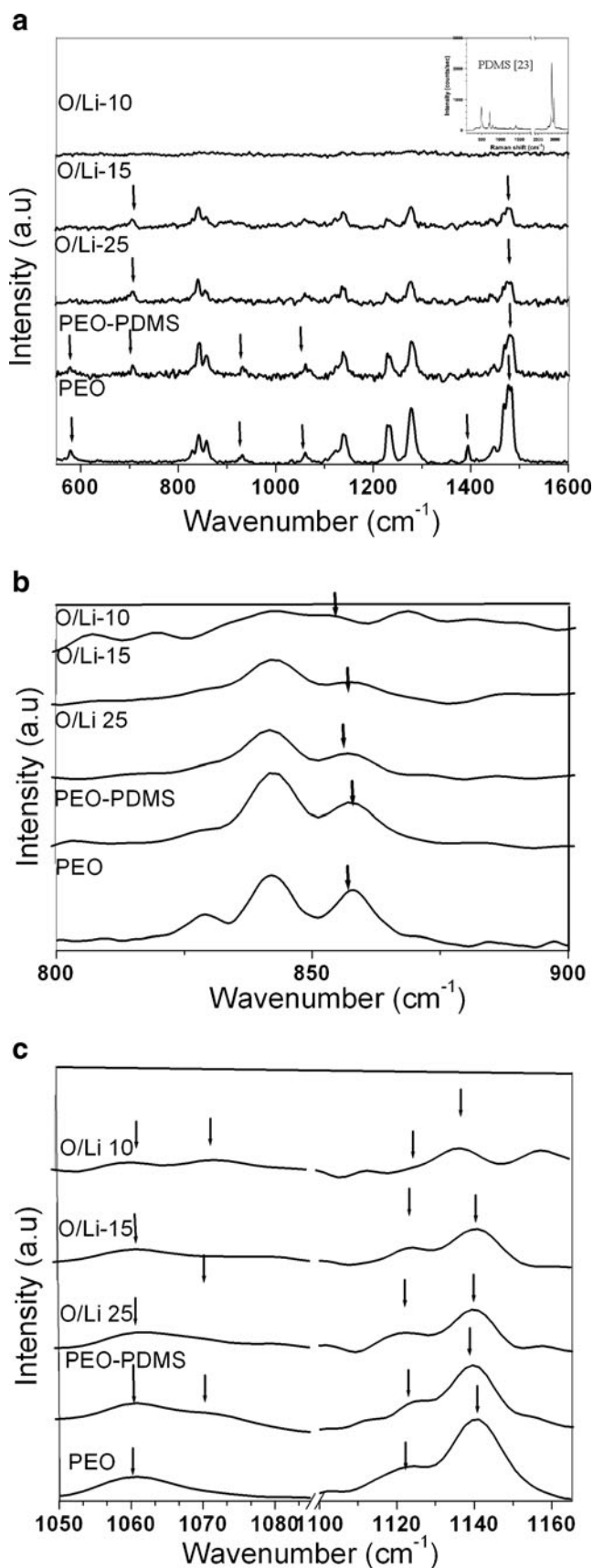
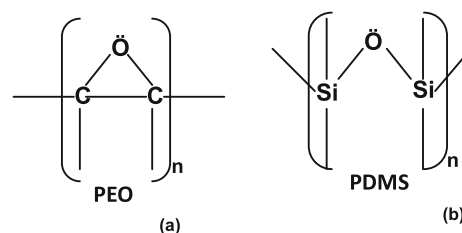


Fig. 5 **a** (i) Raman spectrum for pure PEO, PEO–PDMS (30 % w/w) blend, and blend-based SPE with different O/Li . (ii) Raman spectra of pure PDMS. **b** Raman spectrum of selected bands for pure PEO, PEO–PDMS (30 % w/w) blend, and blend-based SPE with different O/Li . **c** Raman spectrum of CO and CC stretching bands for pure PEO, PEO–PDMS (30 % w/w) blend, and blend-based SPE with different O/Li . [23]

different salt concentrations in the SPE are presented in Table 1. A comparison of the d and R parameters of complexed polymer blend salt system with that of pure PEO and PEO–PDMS blend indicates a systematic increase of interchain separation (i.e., 5.748 to 5.850 Å) and d -spacing (4.598 to 4.680 Å) with increasing salt concentration. These results clearly suggest: (1) interaction of polymer blend matrix with salt, (2) a sequential change in the structural parameters of the host polymer matrix that depends on salt concentration, and (3) increase in the degree of disorder in the polymer blend matrix with increasing salt concentration up to an optimum limit of the salt loading in the matrix.

However, the XRD results do not provide any evidence about the actual site of Li^+ (salt) interaction out of the two polymer components (i.e., whether Li^+ salt interaction occurs at the electron-rich side of the PEO or PDMS as shown below):



In order to confirm it, Raman spectrum analysis of the samples under study has been carried out. The results are described in a subsequent section.

Scanning electron microscopy analysis

Microstructure and surface morphology of the blend polymer–salt system has been studied by SEM shown in Fig. 3a–f. Surface morphology of pure PEO is different from PEO–PDMS blend. Pure PEO clearly shows its characteristic texture and porous microstructure. On the other hand, PEO–PDMS blend exhibits changes in microstructure noticed in the form of spherulites coupled with porosity as usual. The changes clearly indicate PEO–PDMS blend formation. Inclusion of LiPF_6 salt in the blended polymer matrix modulates the surface microstructure of the blend that is clearly visible in Fig. 3c–f. It is noted that porous microstructure of the polymer–salt complex system decreases with increasing salt concentration. The same is true for the surface roughness that is indicated by progressive lowering of the spherulitic texture when compared with that of the PEO–PDMS. The

observed features indicate an increased amorphous content on polymer–salt complexation. The results and changes therein seem to be consistent with earlier reports [13].

Thermal analysis

Figure 4a and b presents differential scanning calorimetry (DSC) results of the host polymer blend (PEO–PDMS (30 % w/w)) and blend-based SPEs with different salt compositions. These results have been compared with the DSC pattern of the PEO, the major component of the host polymer blend (i.e., PEO–PDMS) in order to observe the effect of blending with PDMS on thermal and thermodynamic structural phase composition of the PEO.

The DSC thermogram displayed in the range –70 to 100 °C (Fig. 4a) clearly indicates sharp endotherm at 72 °C representing crystalline to amorphous phase transition of PEO that is well known in literature. On inclusion of PDMS (30 % w/w w. r. t PEO), a small shift in crystalline melting temperature (T_m) of PEO has been noted from 72 to 69 °C. In addition, a clear shoulder in the crystalline melting peak of PEO–PDMS has also been noted at 67 °C. The two melting peaks at 69 °C (T_{m1}) and 67 °C (T_{m2}) are, in fact, partially overlapped (shown in inset of Fig. 4a). They are attributed to the melting of the crystalline part of PEO and PEO–PDMS blend, respectively. However the effect of blending has lowered the standard crystalline melting temperature of pure PEO, the major component of the PEO–PDMS blend.

Upon addition of LiPF₆ salt in different stoichiometric ratios (expressed in terms of the ratio \ddot{O}/Li given in Eq. 1), PEO–PDMS blend has shown noticeable changes in the two crystalline melting peaks with change in \ddot{O}/Li ratio. Since area of the crystalline melting peaks in DSC thermograms gives a direct measure of enthalpy, the changes in crystalline

melting peak attributed to PEO on blending with PDMS and complexation with salt would provide a general idea of thermal stability limit, structural phase (crystalline/amorphous) composition, and other thermodynamic properties, such as enthalpy, etc. These properties are noted from experimental results for different samples under study and presented in Table 2. A comparison suggests a relative decrease in crystallinity of PEO on blending with PDMS that is further lowered on complexation with salts and increase in salt concentration. This observation from DSC appears to be in excellent agreement in the changes in intensity of XRD peaks attributed to PEO in the PEO–PDMS blend (Fig. 2a). Further, the changes in glass transition temperature have also been noted with PDMS blending of PEO and further complexation of the blend. To observe the changes in T_g , we have expanded the DSC thermogram in the limit –70 to –20 °C (Fig. 4b).

Figure 4b indicates a step change at –58 °C for PEO. This has been identified as glass transition temperature of PEO and it is very close to T_g of PEO reported earlier in literature. On inclusion of PDMS (30 % w/w), two distinct step changes are clearly visible in the DSC thermogram (Fig. 4b) observed at –46 and –39 °C. It is to be noted that these step changes, which may be attributed to the glass transition temperatures of the host PEO and PEO–PDMS blend, are higher than the T_g of pure PEO. The results, therefore, indicate that inclusion of PDMS causes drastic changes in the softening property of PEO–PDMS blend. Finally, complexation with salt causes a systematic change in T_g that may favor better flexibility of polymer chain motion in the subambient temperature limits on cation coordination with the host polymer. Hopefully, the changes in T_g may be expected to assist ionic conductivity in the SPE. However, it remains to be seen in the conductivity result that is described subsequently.

Table 3 Raman band position and their assignment for pure PEO, PEO–PDMS, and blend-based solid polymer electrolyte with different \ddot{O}/Li . γ = rocking, τ = twisting, ν = stretching, ω = wagging

Observed Raman band position (cm ⁻¹)	Assignment	Corresponding polymer	Reference	% change in normalized intensity ratio of the Raman bands with host polymer as the reference				
				PEO	PEO–PDMS	\ddot{O}/Li -25	\ddot{O}/Li -15	\ddot{O}/Li -10
707	Si-C	PDMS	[23]	–	100	110	100	20
828 (W)	Not assigned	PEO	[22]	100	83	75	66	25
843 (VS)	$\gamma CH_2 + \nu CO$	PEO	[22]	100	126	74	74	11
857 (S)	$\gamma CH_2 + \nu CO$	PEO	[22]	100	110	50	50	11
1,139 (S)	νCO	PEO	[22]	100	67	67	67	11
1,229 (M)	τCH_2	PEO	[22]	100	50	25	25	10
1,235 (M)	τCH_2	PEO	[22]	100	50	25	25	10
1,278 (VS)	τCH_2	PEO	[22]	100	60	40	40	10
1,394(W)	$\omega CH_2 + \tau CC$	PEO	[22]	100	50	58	58	5

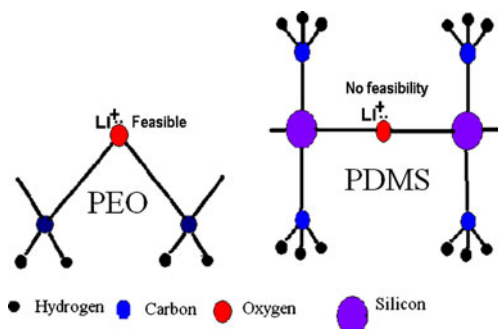


Fig. 6 The C=O site of PEO chain seems to be the most favored site for Li^+ coordination

Raman analysis

Figure 5a shows normalized Raman spectra of pure PEO, PEO–PDMS blend, and blend-based SPE with various salt stoichiometry (i.e., $\bar{O}/\text{Li} \sim 10, 15,$ and 25). The characteristic Raman band assignment has been made in Table 3 that appears to be consistent with previous literature reports [22, 23]. The Raman spectrum of pure PDMS published earlier [23] has been put as inset in Fig. 5a for comparison. Inclusion of PDMS in the PEO matrix causes a general lowering in the intensity of almost all the PEO Raman bands

assigned in Table 3. A comparison indicates that Raman bands of PEO, i.e., CH_2 twisting peaks at $1,235$ and $1,278 \text{ cm}^{-1}$, exhibit significant intensity lowering on inclusion of PDMS in the PEO matrix. On the other hand, C=O stretching vibration of PEO occurring at $1,139 \text{ cm}^{-1}$ and $\gamma(\text{CH}_2) + \nu(\text{CO})$ coupled vibration of PEO occurring at 857 and 843 cm^{-1} show an increase in intensity with PDMS addition. In addition, new changes in the spectrum also appeared. They are: (1) appearance of a new Raman band at 707 cm^{-1} , (2) vanishing of a small shoulder at $\sim 828 \text{ cm}^{-1}$ attributed to PEO (Fig. 5b), and (3) disappearance of $\sim 1,394 \text{ cm}^{-1}$ peak of PEO and intensity lowering of 580 cm^{-1} band. These changes suggest a strong interaction between PEO and PDMS components of the blend (PEO–PDMS) and confirm their blending. It is also to be noted at this stage that origin of Raman peak intensity lies in the change in polarizability or/and mode of phonon vibration. So, a change in the CH_2 and CO peak intensity on inclusion of PDMS evidently indicates that the possibility of blending between the two polymers (PEO and PDMS) is favored.

Further, CH_2 twisting and CO stretching band of PEO exhibits drastic lowering in intensity (Table 3) when LiPF_6 salt is added into the PEO–PDMS blend. This result suggests a very strong interaction between the salt component

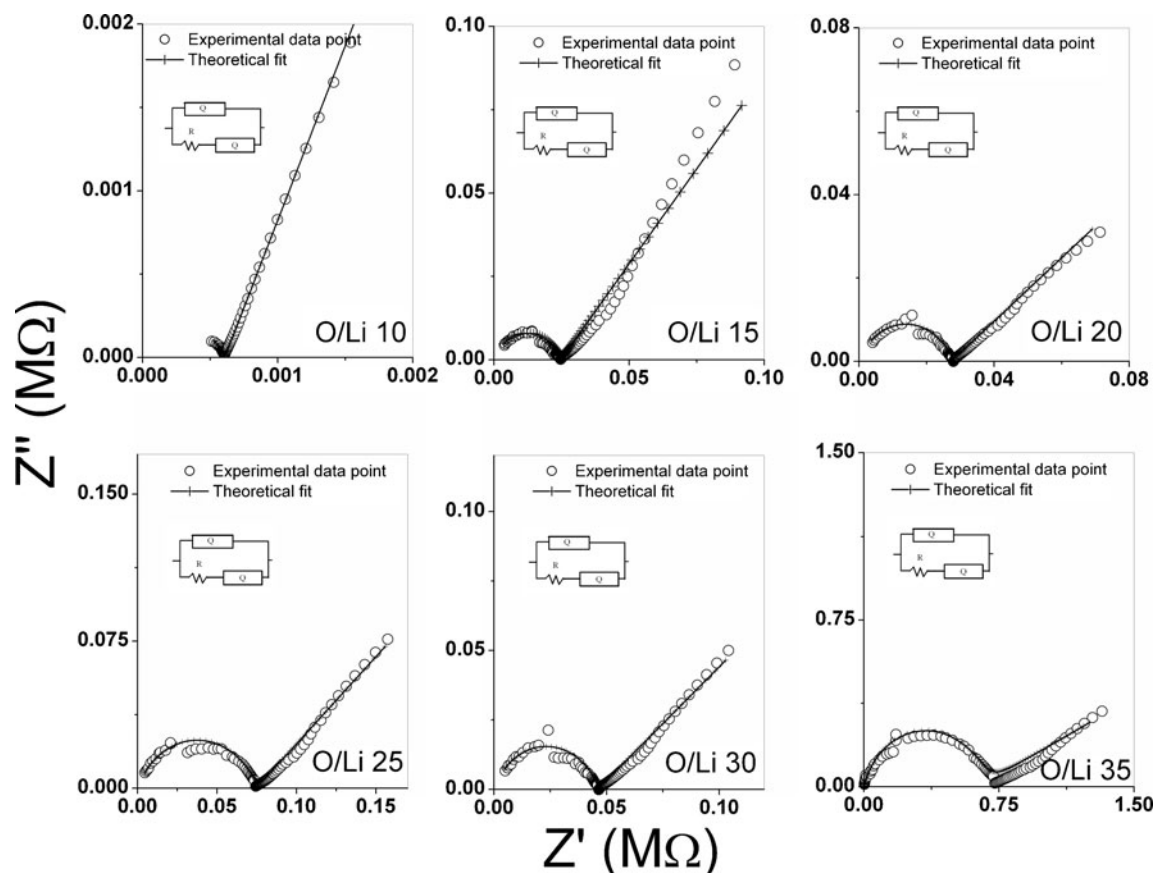


Fig. 7 Impedance plot of PEO–PDMS (30 % w/w)– LiPF_6 with \bar{O}/Li 10, 15, 20, 25, 30, and 35 at room temperature ($30 \text{ }^\circ\text{C}$)

Table 4 Variation of electrical parameter of SPE with \ddot{O}/Li -35, 30, 25, 20, 15, and 10

	\ddot{O}/Li 35	\ddot{O}/Li 30	\ddot{O}/Li 25	\ddot{O}/Li 20	\ddot{O}/Li 15	\ddot{O}/Li 10
R (Ω)	6.4×10^4	4.6×10^4	7.4×10^4	2.7×10^4	7.7×10^4	6.0×10^2
Q_1	2.9×10^{-10}	9.5×10^{-10}	1.1×10^{-9}	1.7×10^{-9}	5.9×10^{-10}	9.8×10^{-9}
n	8.1×10^{-1}	7.5×10^{-1}	7.3×10^{-1}	7.3×10^{-1}	7.3×10^{-1}	6.8×10^{-1}
Q_2	1.6×10^{-6}	1.6×10^{-5}	1.1×10^{-5}	2.3×10^{-5}	4.0×10^{-6}	2.1×10^{-5}
n	2.7×10^{-1}	4.3×10^{-1}	4.6×10^{-1}	4.1×10^{-1}	5.4×10^{-1}	7.1×10^{-1}
C_{dl} (F) at 100 kHz	3.6×10^{-11}	7.5×10^{-11}	6.5×10^{-11}	1.4×10^{-10}	1.5×10^{-10}	3.4×10^{-8}
C_{dl} (F) at 10 Hz	3.4×10^{-7}	3.2×10^{-6}	2.3×10^{-6}	4.0×10^{-6}	3.2×10^{-6}	7.4×10^6

and the host polymer blend. Since $C=\ddot{O}$ of the PEO has a lone pair of electron, Li^+ coordination with the PEO backbone appears to be the most likely and favored possibility. In order to augment the above-mentioned observation and corroborate it further for confirmation of the actual Li^+ coordination site in the polymer blend matrix, profile of $C=\ddot{O}$ stretching bands has been examined for pure PEO, PEO–PDMS, and SPE with different salt concentrations in Fig. 5b and c. A comparison indicates that polarizability of $C=\ddot{O}$ bond of the $\gamma CH_2 + \nu C=\ddot{O}$ coupled oscillation has undergone a change on complexation with Li^+ . As a result,

incident laser energy interacts differently with the CO bond vibrational mode causing substantial intensity change. Since, Si–O–Si vibration mode of PDMS falls below our experimental frequency range, the possibility of Li interaction with Si–O–Si of PDMS could not be examined. However, the Si–C vibration at 707 cm^{-1} attributed to PDMS remained unaltered, suggesting a noninteracting PDMS backbone with Li^+ ion. In the light of evidences noted herein, the $C=\ddot{O}$ site of PEO chain seems to be the most favored site for Li^+ coordination. It is illustrated in Fig. 6.

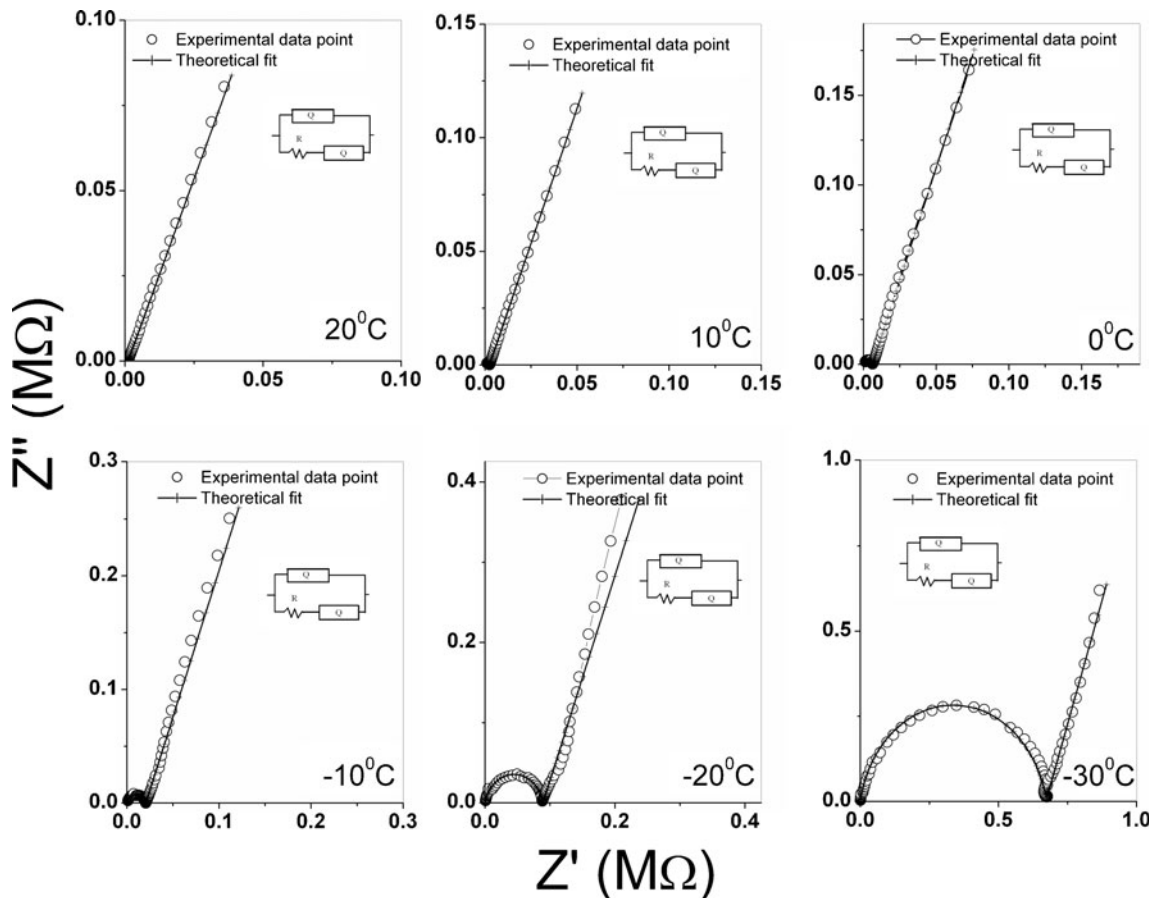


Fig. 8 Impedance plot of PEO–PDMS (30 % w/w)–LiPF₆ (\ddot{O}/Li -10) at different ambient and sub-ambient temperatures

Table 5 Variation of electrical parameter of SPE with $\ddot{O}/Li \sim 10$ at different temperatures

	20 °C	10 °C	0 °C	-10 °C	-20 °C	-30 °C
R (Ω)	1.1×10^3	2.4×10^3	6.2×10^3	2.0×10^4	8.9×10^4	6.7×10^5
Q_1	3.9×10^{-9}	2.9×10^{-9}	1.3×10^{-9}	9.9×10^{-10}	5.4×10^{-10}	2.8×10^{-10}
n	7.5×10^{-1}	7.7×10^{-1}	8.1×10^{-1}	8.3×10^{-1}	8.6×10^{-1}	8.9×10^{-1}
Q_2	1.5×10^{-5}	1.1×10^{-5}	7.5×10^{-6}	5.1×10^{-6}	3.5×10^{-6}	2.1×10^{-6}
N	7.3×10^{-1}	7.4×10^{-1}	7.6×10^{-1}	7.6×10^{-1}	7.6×10^{-1}	7.9×10^{-1}
C_{dl} (F) at 100 kHz	1.2×10^{-8}	3.4×10^{-9}	7.2×10^{-10}	1.9×10^{-10}	9.2×10^{-11}	7.3×10^{-11}
C_{dl} (F) at 10 Hz	5.5×10^{-6}	4.2×10^{-6}	3.2×10^{-6}	2.3×10^{-6}	2.3×10^{-6}	6.7×10^{-7}

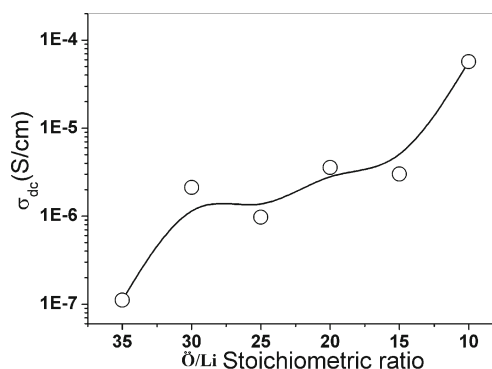
Impedance analysis

Impedance spectrum (IS) studies were carried on the samples with different stoichiometry of salt in the polymer blend (PEO–PDMS) over a range of temperature in the limits ± 30 °C in order to evaluate electrical properties. Figure 7 shows Nyquist plot of SPE films with varying salt concentrations (\ddot{O}/Li) at room temperature. The Nyquist plot exhibits a high frequency semicircular arc that is followed by another arc attributed to a large semicircle. This typical feature is invariably common in the SPE with \ddot{O}/Li loading varying in the limits 35 (low salt content) to a progressive increasing salt concentration ($\ddot{O}/Li \sim 20$). The high-frequency semicircle is attributed to the bulk property, whereas the low-frequency second arc may be related to either grain/phase boundary or interfacial phenomena. With further rise in salt concentration ($\ddot{O}/Li \sim 15$), the radius of curvature of the high-frequency semicircular arc is reduced, whereas the second arc in the low-frequency region takes the shape of a spike. A lowering in the radius of curvature of the high-frequency arc suggests lowering of resistivity with increasing salt concentration. This is also corroborated by the presence of spike that arises due to an effective accumulation of fast ion transport at the interfacial boundaries of the cell: Au || SPE || Au, with blocking (Au) electrodes. The presence of spike is a very dominating feature for a sample with $\ddot{O}/Li \sim 10$. It suggests that rate of ion migration on application of electrical stimuli is very large, causing predominant charge accumulation at the interface with blocking electrode. The overall picture from the analysis described above suggests that the SPE sample with salt composition in the ratio $\ddot{O}/Li \sim 10$ exhibits faster ion transport with the possibility of high electrical conductivity. This aspect has been discussed later in the manuscript.

The electrical response of the SPE films, noted in terms of complex IS (CIS) plot, has been modeled by an electrical equivalent circuit (shown in the inset) for SPE samples of different \ddot{O}/Li . The equivalent circuit modeling suggests excellent agreement between theoretical response (solid line) and experimental results (data points). The electrical parameters for different SPE, obtained from equivalent

circuit analysis, are presented in Table 4. A comparison indicates that bulk resistance is the minimum in the case of SPE with $\ddot{O}/Li \sim 10$. This composition, prima facie, may be expected to have better electrical conductivity among the series under investigation. Therefore, the electrical response of this particular composition has only been investigated in subambient temperature limit varying from -30 to $+30$ °C.

Figure 8 depicts CIS spectrum of SPE with $\ddot{O}/Li \sim 10$ in the ambient and subambient temperature limits. It is clearly visible that CIS response of this sample exhibits markedly visible difference at low temperatures when compared with its room-temperature Nyquist plot. At -30 °C and above (up to 0 °C), this sample exhibits a typical IS comprising of a high-frequency region at -30 °C. The low-frequency arc slowly turns into a spike with rise in temperature up to 0 °C, as expected. The result provides clear indication of separable bulk and grain/phase boundary phenomena in the subambient temperature limit up to 0 °C with additional information of increase in the ionic transport with progressive rise in the temperature (i.e., via reduced radius of curvature and progressively strengthened spike in the low-frequency region as temperature changes from -30 to 0 °C). With further rise in temperature, the semicircular arc appears to be masked, whereas a low-frequency spike becomes very predominant. The origin of the latter lies in large accumulation of ionic charge carriers at the interface of SPE-

**Fig. 9** Conductivity vs. salt concentration of PEO–PDMS (30 % w/w)–LiPF6 at room temperature (30 °C)

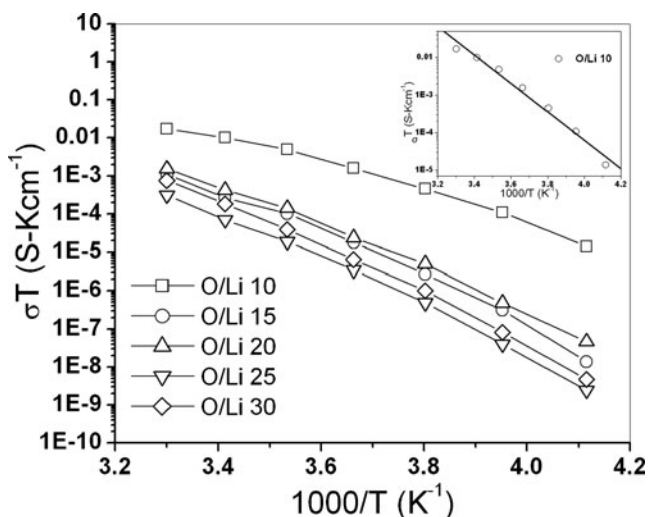


Fig. 10 Conductivity vs. temperature plot of PEO–PDMS (30 wt.%)–LiPF6 (Ö/Li ~10-30)

blocking electrode possibly due to faster ion dynamics. This has, in fact, been found to be reasonable and convincing when electrical parameters were obtained at different temperatures by electrical equivalent circuit modeling of the experimental impedance results. The corresponding equivalent electrical circuit has been shown as an inset and the magnitudes of the electrical parameters at different temperatures are given in Table 5. A comparison indicates very clearly from the values of bulk resistance (R_b) and double layer capacitance (C_{dl}) that our inference is logical and convincing. The DC conductivity of the SPE films in the present studies has been evaluated from the CIS. The bulk resistance (R_b) is obtained by noting down the value of intercept of high-frequency semicircular arc (first arc) on the real (Z') axis of the Nyquist plot.

Figure 9 shows variation of bulk (DC) conductivity (σ_{dc}) of the blend polymer-based SPEs as a function of salt concentration at room temperature (30 °C). The pattern of conductivity variation indicates that at lower salt concentration (i.e., Ö/Li ~35) in the host polymer blend, σ_{dc} , is very low ($\sim 10^{-7}$ S cm $^{-1}$). However, the magnitude of σ_{dc} appears to increase with rise in the salt concentration up to a limiting concentration (Ö/Li ~10). The jump in conductivity with

change in salt concentration is large (i.e., ~3 orders of magnitude). SPE with salt concentration higher than this (i.e., Ö/Li > ~8 or 5) could not be obtained in solid (free-standing) form. So, the SPE with Ö/Li ~10 has been observed to be optimized composition in the present studies.

Further, an enhancement in the σ_{dc} with increase in salt concentration appears well in accordance with the relation; $\sigma_{dc} = nq\mu$, where n = no. of mobile charge carriers, q = charge, and μ = mobility. Assuming complete dissociation of salt in the SPE matrix, the parameter n is likely to have larger value with increase in the salt concentration in SPE. Hence, the enhancement in conductivity with increase in the salt concentration is a natural consequence. Subjected to the validity of the assumption made herein, a similar result has also been reported in literature for PVDF–LiPF $_6$ system by Chiang et al. [24], and when compared with the DC conductivity of PEO–salt system [10–12] or with pure PEO [25], the reported conductivity in the present studies appears to be a very large enhancement. Such a comparison with earlier reports has also been shown in Fig. 1b. The highest DC conductivity, obtained for the optimized composition in the present work, is 5.7×10^{-5} S cm $^{-1}$ at 30 °C that is lower by an order/factor of 3 when compared with $\sigma_{dc} \sim 10^{-8}$ S cm $^{-1}$ at –30 °C. This high ionic conductivity at ambient and subambient temperatures appears to be in good co-relation with DSC observation.

A variation of DC conductivity with temperature has been shown in Fig. 10. It shows an Arrhenius-type behavior. It indicates that ion motion in the optimized SPE composition exhibits a thermally activated process. Activation energy has also been calculated by fitting the temperature-dependent conductivity results in accordance with the Arrhenius equation: $\sigma = \sigma_0 e^{-\frac{E_a}{kT}}$. The details of the conductivity parameters are shown in Table 6. Conductivity of the system under study has been compared with existing literature reports in Table 7. A comparison of the results indicates that ion conduction in the polymer–salt system is primarily dominated by local motion of the polymer chain. So, such systems invariably show good conductivity at higher temperature, preferably well above T_g . At higher temperatures (i.e., $T \geq T_g$), polymer segmental motion is more favorable, thereby augmenting faster ion dynamics and enhanced

Table 6 DC conductivity and activation energy for different SPEs at ambient and subambient temperature

Sample name	σ_{dc} (S cm $^{-1}$) at 30 °C	σ_{dc} (S cm $^{-1}$) at 0 °C	σ_{dc} (S cm $^{-1}$) at –10 °C	σ_{dc} (S cm $^{-1}$) at –20 °C	σ_{dc} (S cm $^{-1}$) at –30 °C	E_a (eV)
PEO–PDMS (30 wt.%)–LiPF $_6$ (Ö/Li-10)	5.7×10^{-5}	5.7×10^{-6}	1.7×10^{-6}	4.3×10^{-7}	5.7×10^{-8}	0.32
PEO–PDMS (30 wt.%)–LiPF $_6$ (Ö/Li-15)	3.6×10^{-6}	6.5×10^{-8}	1.0×10^{-8}	1.2×10^{-9}	5.6×10^{-11}	0.5
PEO–PDMS (30 wt.%)–LiPF $_6$ (Ö/Li-20)	5.0×10^{-6}	8.7×10^{-8}	1.9×10^{-8}	1.9×10^{-9}	1.9×10^{-10}	0.47
PEO–PDMS (30 wt.%)–LiPF $_6$ (Ö/Li-25)	9.7×10^{-7}	1.3×10^{-8}	1.8×10^{-9}	1.6×10^{-10}	9.9×10^{-12}	0.53
PEO–PDMS (30 wt.%)–LiPF $_6$ (Ö/Li-30)	2.5×10^{-6}	2.3×10^{-8}	3.9×10^{-9}	3.2×10^{-10}	1.9×10^{-11}	0.54

Table 7 Conductivity comparison of different electrolytes at ambient and subambient temperatures

Nature of electrolyte	Samples	Ambient temperature		Subambient temperature				Reference	
		30 °C	20 °C	0 °C	−10 °C	−20 °C	−30 °C		
Liquid electrolyte	LiPF ₆ –EC–DEC–EP	10 ^{−2}	10 ^{−3}	10 ^{−3}	10 ^{−3}	10 ^{−3}	10 ^{−3}	4	
	LiPF ₆ –EC–DMC–EMC	10×10 ^{−3}	–	4×10 ^{−3}	–	>2×10 ^{−3}	2×10 ^{−3}	1	
	LiPF ₆ –EMC	4×10 ^{−3}	–	2×10 ^{−3}	–	2×10 ^{−3}	<2×10 ^{−3}	1	
	LiPF ₆ –EC–DMC	10×10 ^{−3}	–	6×10 ^{−3}	–	2×10 ^{−3}	2×10 ^{−3}	1	
	0.6 M [TPFPB] + LiF + PC:DMC	–	3.2×10 ^{−3}	–	–	1.2×10 ^{−3}	–	2	
	THFPB + LiF + PC + DMC	–	3.3×10 ^{−3}	–	–	0.8×10 ^{−3}	–	2	
	1 M LiBF ₄ + PC + DMC	–	4.9×10 ^{−3}	–	–	1.8×10 ^{−3}	–	2	
	1 M LiPF ₆ + EC + DMC	–	8.8×10 ^{−3}	–	–	0.58×10 ^{−3}	–	2	
	1 M–LiTFSi–EC–DMC–EMC	10×10 ^{−3}	–	–	5×10 ^{−3}	–	3×10 ^{−3}	26	
	1 M LiBOB–PC–EC–EMC	10 ^{−3}	–	–	10 ^{−3}	–	10 ^{−4}	3	
	1 M LiPF ₆ –EC–PC–EMC	10 ^{−2}	–	–	10 ^{−3}	–	10 ^{−3}	5	
	Solid polymer electrolyte	PDMS–co-PEO + LiCLO ₄	2.6×10 ^{−4}	–	–	–	–	3×10 ^{−5}	16
		PVDF–LiCLO ₄	10 ^{−8}	10 ^{−8}	10 ^{−9}	10 ^{−10}	−10 ^{−10}	–	18
PEO–LiCLO ₄		10 ^{−6}	10 ^{−7}	10 ^{−8}	10 ^{−8}	10 ^{−9}	–	18	
PVDF–HFP–LiPF ₆		10 ^{−7}	10 ^{−8}	10 ^{−8}	10 ^{−8}	10 ^{−8}	–	18	
PVDF–HFP–LiCl		10 ^{−9}	10 ^{−9}	10 ^{−9}	10 ^{−9}	−10 ^{−9}	–	18	
PVDF–HFP–LiBETi		10 ^{−5}	10 ^{−5}	10 ^{−6}	10 ^{−6}	10 ^{−6}	–	18	
Solid polymer electrolyte under study	PEO–PDMS (30 wt.%)–LiPF ₆ (Ö/Li-10)	5.7×10 ^{−5}	–	5.7×10 ^{−6}	1.7×10 ^{−6}	4.3×10 ^{−7}	5.7×10 ^{−8}	System under report	
	PEO–PDMS (30 wt.%)–LiPF ₆ (Ö/Li-15)	3.6×10 ^{−6}	–	6.5×10 ^{−8}	1.0×10 ^{−8}	1.2×10 ^{−9}	5.6×10 ^{−11}		

conductivity, whereas at subambient temperature ($T \leq T_g$), ion mobility reduces due to increase in the polymer stiffness, causing internal friction and resistance to chain motion. An enhancement in σ_{dc} in the present studies is attributed to inclusion of very low T_g polymer (i.e., PDMS) into another polymer having low T_g (i.e., PEO). Since PDMS has very low T_g and a gelly-type structure at room temperature, it reduces local viscosity and internal friction providing a liquidlike pathway for ion migration in the PEO–PDMS-blended matrix. The overall result is enhanced conductivity.

Ion transport analysis

Using Wagner's DC polarization technique, ion transport number (t_{ion}) of the optimized (Ö/Li ~10) blend polymer–salt complex has been evaluated at room temperature (27 °C) with an applied DC bias ~50 mV across the sample cell (SS || SPE || SS). Polarization current vs. time (Fig. 11) shows typical characters of a predominantly ionic conductor. Initially, the

current shows a very high value followed by a sudden fall and reaches saturation. The initial current (I_t) is due to ionic and electronic charged species and the saturated current value is

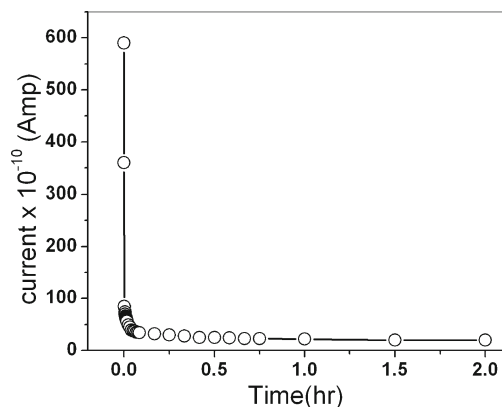


Fig. 11 Ion transport of PEO–PDMS (30 % w/w)–LiPF₆(Ö/Li ~10) at room temperature

attributed to only electronic (I_e). Transport no. has been calculated by using the following relation:

$$t_{\text{ion}} = \frac{I - I_e}{I} \times 100 \quad (3)$$

$$t_{\text{ion}} + t_e = 1$$

The optimized blend polymer electrolyte ($\ddot{\text{O}}/\text{Li} \sim 10$) sample shows 97 % ionic transport at room temperature, which is in the desirable limit for energy storage device applications.

Summary and conclusion

PEO–PDMS blend-based SPE has been prepared and optimized with respect to salt concentration and low temperature ionic conductivity. The observed experimental results on the blend-based polymer electrolyte shows that: (1) a drastic change in the surface property and morphology with inclusion of salt into the PEO–PDMS blend has taken place, whereas the XRD results confirm an effective interaction between the polymer matrix and the electropositive cation component of the salt; (2) Li^+ ion coordination only at the $\text{C}=\ddot{\text{O}}$ site of the PEO has been successfully established by the Raman spectroscopy results; and (3) an optimized ($\ddot{\text{O}}/\text{Li} \sim 10$) SPE shows room temperature (30 °C) conductivity as high as $5.7 \times 10^{-5} \text{ S cm}^{-1}$ that changes to $5.7 \times 10^{-6} \text{ S cm}^{-1}$ at 0 °C and remains almost the same in the subambient temperature limit up to -10 °C.

It is concluded that a blend-based SPE may be suitable as a plastic separator even in the ambient and subambient temperature limits with further scope of improvement in ionic conductivity on composite formation.

Acknowledgments The authors acknowledge with thanks the financial support received from the Armament Research Board (ARMREB), DRDO, Govt. of India, New Delhi, for financial support to carry out this piece of work under grants-in-aid scheme. Thanks are also due to Prof. A. K. Bhowmick, Director IIT Patna, for encouragement and support in all respect. The use of facilities availed at the Department of Physics and Meteorology at IIT Kharagpur is also acknowledged gratefully.

References

- Pelchita EL, Bahel WK (2000) A low-temperature electrolyte for lithium and lithium-ion batteries. *J Power Sources* 88:192–196
- Li LF, Lee HS, Li H, Yang XQ, Nam KW, Yoon WS, Mc Breen J, Huang XJ (2008) New electrolytes for lithium ion batteries using LiF salt and boron based anion receptor. *J Power Sources* 184:517–521
- Zhang SS (2006) A unique lithium salt for the improved electrolyte of Li-ion battery. *Electrochem Commun* 8:1423–1428
- Kufian MZ, Majid SR (2010) Performance of lithium-ion cells using M LiPF₆ in EC/DEC ($v/v = 1/2$) electrolyte with ethyl propionate additive. *Ionics* 16:409–416
- Zhang SS, Xu K, Jow TR (2002) A new approach toward improved low temperature performance of Li-ion battery. *J Electrochem Commun* 4(11):928–932
- Tikhonov K, Kosh VR Li-ion battery electrolytes designed for a wide temperature range. Woburn, MA01801, Covalent associates, Inc. www.covalentassociates.com
- Manual Stephan A (2006) Review on gel polymer electrolytes for lithium batteries. *Eur Polym J* 42:21–42
- Min HS, Kang DW, Lee DY, Kim DW (2002) Gel polymer electrolytes prepared with porous membranes based on an acrylonitrile/methyl methacrylate copolymer. *J Polym Sci B* 40:1496–1502
- Wieczorek W, Floarjanczyk Z, Zukowska G, Borkowska R, Kuzma P, Monikowska EZ, Kuzwa K (2002) Ambient and sub-ambient temperature proton conducting polymer gel electrolytes. *Solid State Ionics* 154–155:45–49
- Ibrahim S, Johan MR (2012) Thermolysis and conductivity studies of poly(ethylene oxide) (PEO) based polymer electrolytes doped with carbon nanotube. *Int J Electrochem Sci* 7:2596–2615
- Magistrisetal A, Mustarelli P, Quartarone E, Tomasi C (2000) Transport and thermal properties of (PEO)_n-LiPF₆ electrolytes for super-ambient application. *Solid State Ionics* 136–137:1241–1247
- Stoeva Z, Litas IM, Staunton E, Andreev YG, Bruce PG (2003) Ionic conductivity in the crystalline polymer electrolytes PEO:LiXF₆, X = P, As, Sb. *J Am Chem Soc* 125:4619–4626
- Lee JY, Bhattacharya B, Kim DW, Park JK (2008) Poly(ethylene oxide)/poly (dimethyl siloxane) blend based solid polymer electrolyte and its dye synthesized solar cell applications. *J Phys Chem C* 112:12576–12582
- Lobtiz P, Fullbier H, Reiche A, Illner JC (1992) Ionic conductivity in poly (ethylene oxide)–poly (alkylmethacrylate)–block copolymer mixtures with LiI. *Solid State Ionics* 58:41–48
- Livshits E, Kovarsky R, Lavie N, Hayashi Y, Golodnitsky D, Peled E, Livshitsetal E (2005) New insight in to structural and electrochemical properties of anisotropic polymer electrolytes. *Electrochim Acta* 50:3805–3814
- Fonseca CP, Neves S (2002) Characterization of polymer electrolytes based on poly (die methyl siloxane-co-ethylene oxide). *J Power Sources* 104:85–89
- Johnstone C, Hooper A, Pethrick RA (1990) Polymer electrolyte based on a dimethyl siloxane-polyethylene oxide copolymer. *Eur Polym J* 26:987–990
- Fan LZ, Wang XL, Long F (2009) All solid state polymer electrolyte with plastic crystal materials for rechargeable lithium ion battery. *J Power Sources* 189:775–778
- Walker CN, Versek C, Touminen M, Tew GN (2012) Tunable network from thiolene chemistry for lithium ion conduction. *ACS Macro Lett* 1:732–741
- Shukla N, Thakur AK (2009) Role of salt concentration on conductivity optimization and structural phase separation in a solid polymer electrolyte based on PMMA-LiCLO₄. *Ionics* 15:357–367
- Mihaylova MD, Kretev VP, Krestava MN, Amzil A, Berlinova IV (2001) Amphiphilic graft copolymers with poly(oxy ethylen) side chains: supermolecular structure in solid state: I. WAXS studies. *Eur Polym J* 37:233–239
- Capiglia C, Imanishi N, Takeda Y, Henderson WA (2003) Poly (ethylene oxide) LiN(SO₂CF₂CF₃)₂ polymer electrolytes IV. Raman characterization. *J Electrochem Soc* 150(4):A525–A531
- Bal SC, Lee H, Lin Z, Granick S (2005) Chemical imaging in a surface force apparatus: confocal Raman spectroscopy of confined poly(diemethyl siloxane). *Langmuir* 21:5685–5688
- Chiang CY, Shen YJ, Reddy MJ, Chu PP (2003) Complexation of poly(vinylidene fluoride): LiPF₆ solid polymer electrolyte with enhanced ion conduction in ‘wet’ form. *J Power Sources* 123:222–229
- Dygas JR, Faraj BM, Florjanczyk Z, Krok F, Marzantowicz M, Monikowska EZ (2003) Effects of inhomogeneity on ionic conductivity and relaxation in PEO and PEO salt complex. *Solid State Ionics* 157:249–256
- Mandal BK, Padhi AK, Shi Z, Chakraborty S, Filler R (2006) New low temperature electrolytes with thermal runaway in habitation for Li-ion rechargeable battery. *J Power Sources* 162:690–695